

RESEARCH ARTICLE

# Decoupled motion planning of a mobile manipulator for precision agriculture

Giovanni Colucci\* , Luigi Tagliavini , Andrea Botta , Lorenzo Baglieri  and Giuseppe Quaglia 

DIMEAS - Department of Mechanical and Aerospace Engineering, Politecnico di Torino, Torino, Italy  
\*Corresponding author. E-mail: [giovanni\\_colucci@polito.it](mailto:giovanni_colucci@polito.it)

**Received:** 15 November 2022; **Revised:** 17 January 2023; **Accepted:** 13 February 2023;

**First published online:** 16 March 2023

**Keywords:** precision agriculture, SDG 12, mobile robots, service robots, inverse kinematics

## Abstract

Thanks to recent developments in service robotics technologies, precision agriculture (PA) is becoming an increasingly prominent research field, and several studies were made to present and outline how the use of mobile robotic systems can help and improve farm production. In this paper, the integration of a custom-designed mobile base with a commercial robotic arm is presented, showing the functionality and features of the overall system for crop monitoring and sampling. To this aim, the motion planning problem is addressed, developing a tailored algorithm based on the so-called manipulability index, that treats the base and robotic arm mobility as two independent degrees of motion; also developing an open source closed-form inverse kinematics algorithm for the kinematically redundant manipulator. The presented methods and sub-system, even though strictly related to a specific mobile manipulator system, can be adapted not only to PA applications where a mobile manipulator is involved but also to the wider field of assistive robotics.

## 1. Introduction

In the past years, precision agriculture (PA) has become a prominent research field, thanks to its significant impact for responsible water resource consumption [1], but also fertilisers, chemicals and pesticides reduction [2, 3]. The increasing population growth rate, which is expected to bring the global population to 9.7 billion by 2050 [4], is leading to a raise in food demand [5–7], especially in developing countries where land was withdrawn from cultivation for cities expansion [8], with a greater exploitation of the fields and mass crops. PA methods are nevertheless devoted to a data-driven approach for responsible and intelligent crops farming, thus pursuing the 2030 Agenda for Sustainable Development, especially the sustainable development goal (SDG) 12 towards sustainable consumption and production patterns [9].

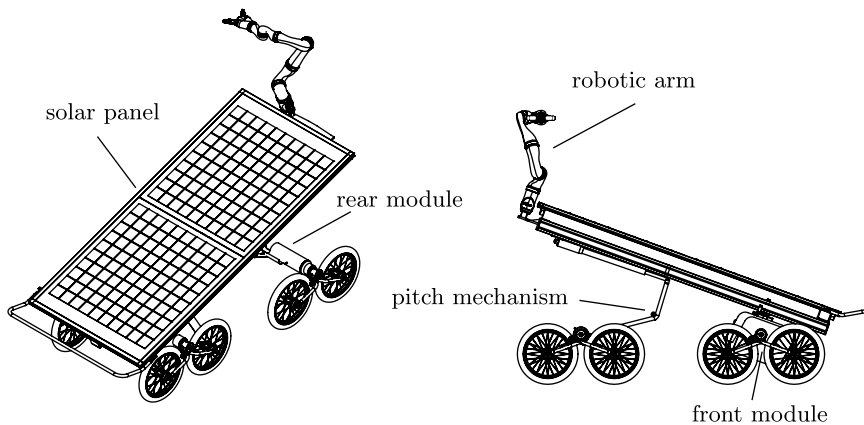
To this aim, a massive scientific activity about the implementation of novel technologies for crops farming was performed in the past decades, especially about integrated mobile systems that are capable of autonomous navigation while monitoring the crops [10–12], or even capable of helping farmers during their activities, e.g. trimming [13–15], spraying [16, 17] and harvesting [18, 19]. All the cited systems are briefly presented in Table I and their main features, e.g. the main purpose and manipulator type, are reported.

To develop a novel UGV (unmanned ground vehicle) for PA purposes, the researchers from Politecnico di Torino had developed the Agri.Q prototype, depicted in Fig. 1, which is a custom mobile manipulator mainly designed for grapevine cultivation [20, 21].

Agri.Q locomotion system is composed of two modules: the front and rear modules, both equipped with two drive motors and four wheels. While the significant number of wheels is fundamental to

**Table I.** Mobile manipulators for precision agriculture.

Study	Purpose	Target	Base	Locomotion	Arm
Strisciuglio N. et al. [13]	Gardening	Rose bush	Commercial	Differential drive	Commercial (6 d.o.f.)
Adamides G. et al. [16]	Spraying	Vineyard	Commercial	Differential drive	Commercial (6 d.o.f.)
Feng Q. et al. [18]	Harvesting	Tomato fruit	Custom	Rail guided	Commercial (4 d.o.f.)
Vinum Project [14]	Pruning	Vineyard	Commercial	Legged	Commercial (7 d.o.f.)
De Preter et al. [19]	Harvesting	Strawberry (greenhouse)	Custom	Differential drive	Custom
Botteril T. et al. [15]	Pruning	Vineyard	Custom	Winch driven	Commercial (6 d.o.f.)
Goričaneč J. et al. [17]	Spraying	Vineyard	Custom	Flipper-tracked	Commercial (7 d.o.f.)

**Figure 1.** The Agri.Q mobile manipulator for Precision Agriculture.

properly distribute the UGV weight on the ground, the all-wheels drive mode is fundamental to navigate in case of steep slopes or uneven terrains. The system is also provided with a photovoltaic panel, which allows the self-charging mode, and it can be properly oriented, thanks to a controlled pitch-roll motion, to exploit the solar radiation, thus maximising the self-charging mode. Moreover, the integration with the Kinova Jaco2 commercial robotic arm makes the system capable of performing few tasks where the interaction with the environment is fundamental, e.g. crop sampling and spraying.

In Fig. 2, the Agri.Q High-Level architecture is presented. The electric energy is stored into a 7S14P Li-Po battery that can be both re-charged by an external supply or the PV panels themselves. The rover can be directly commanded by a human being user through a remote control, whose receiver gives the input commands to the low-level micro-controller that drives the mobile base motors. Alternatively, the mobile base can operate in autonomous mode through the commands provided by an on-board computer, which can also control the robotic manipulator.

Apart from the novelty of the Agri.Q prototype, which was already discussed by the authors within the previously cited works, this article presents the motion planning pipeline that was developed to allow

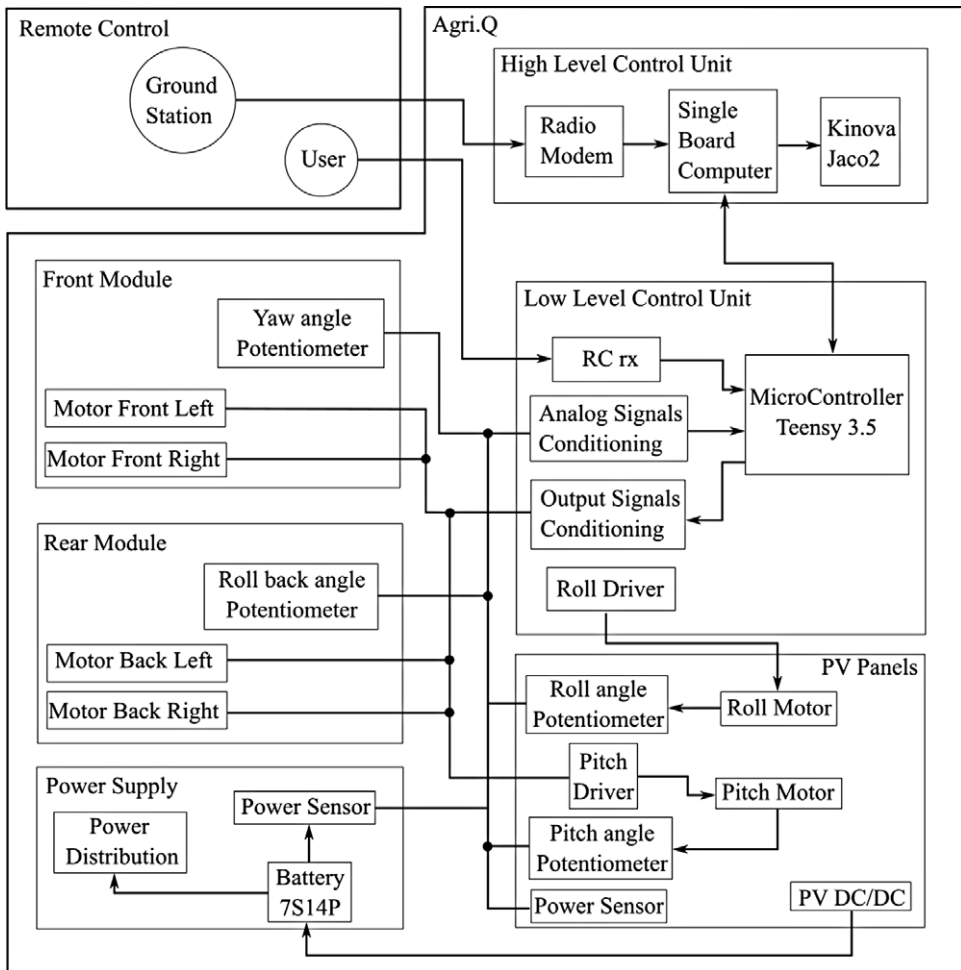


**Figure 2.** High-Level architecture of the Agri.Q mobile manipulator.

Agri.Q to perform simple crop sampling activities, exploiting both the mobile base and the arm mobility. Significant contributions of the paper are specified hereinafter:

- The implementation of a closed-form inverse kinematics algorithm that exploits the elbow redundancy for the Jaco2 manipulator is extensively presented and developed, and it is also provided by the authors as an open-source code for further research activities;
- The whole system motion planning pipeline is reported, presenting also how the decoupling of the base mobility and arm mobility can be used to place the target object of the pick-and-place task inside the area where the arm exhibits its highest manipulation capacities.

The present work is the extended version of the paper presented by the authors at the 31st International Conference on Robotics in the Alpe-Adria-Danube Region [22]. The following chapters are organised as follows:

- Section 2 presents the inverse kinematics of the manipulator and the estimation of the manipulation abilities with the use of a modified version of the manipulability index;
- Section 3 discusses the implementation of the arm kinematics within the whole system motion planning architecture.

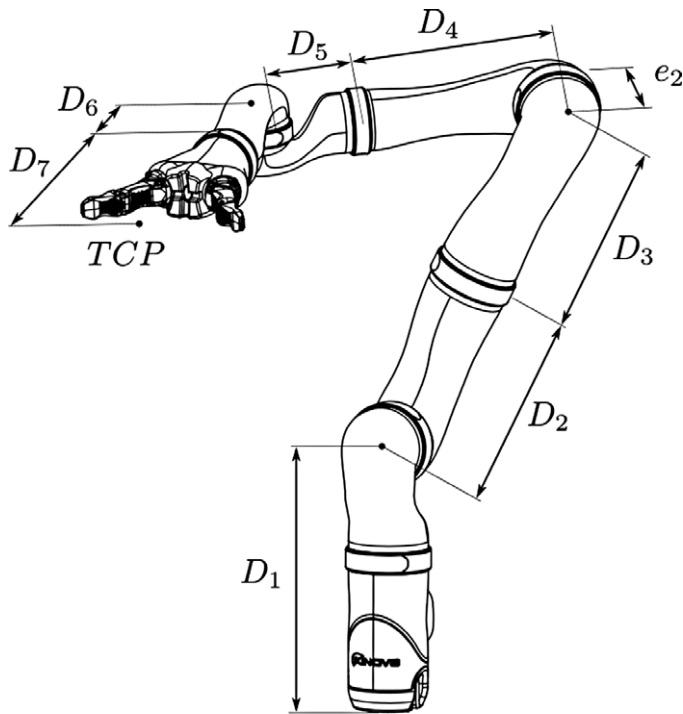


**Figure 3.** Kinova Jaco2 Manipulator and its fundamental geometric properties. The elbow off-set is labelled as  $e_2$ .

**Table II.** Denavit–Hartenberg parameter values for the Jaco2 Manipulator for each  $i$ th reference frame.

$i$	$a_i$	$\alpha_i$	$d_i$	$\theta_i$
1	0	$-\pi/2$	$-D_1$	$q_1$
2	0	$-\pi/2$	0	$q_2$
3	0	$-\pi/2$	$-(D_2 + D_3)$	$q_3$
4	0	$-\pi/2$	$-e_2$	$q_4$
5	0	$-\pi/2$	$-(D_4 + D_5)$	$q_5$
6	0	$-\pi/2$	0	$q_6$
7	0	$-\pi$	$-(D_6 + D_7)$	$q_7$

## 2. Jaco2 Manipulator Inverse Kinematics

The Kinova Jaco2 robotic manipulator can be modelled as a serial kinematic chain composed of eight links and seven revolute joints, where the first link is fixed to the Agri.Q rover and the last one represents the end-effector. In Fig. 3, the Jaco2 manipulator and its geometric properties is presented. It is worth underlining the elbow off-set  $e_2$  inducing a misalignment in the kinematic chain that will be discussed further. Since the arm should operate in a three-dimensional workspace with an arbitrarily defined orientation, its seven degrees of freedom guarantee the kinematically redundancy of the system [23]; thus, for each pose, there are  $\infty^1$  possible solutions to the inverse kinematics problem. The definition of the link frames was performed through the use of the Denavit–Hartenberg convention, even though the coefficient values were slightly modified to make them consistent when commanding the real manipulator, as can be verified by comparing the values in Table II with the parameters in the official documentation [24].

According to the official Kinova documentation, the fixed homogeneous transformation matrix that sets  $\{0\}$  with respect to  $\{b\}$  is the following:

$$\mathbf{T}_0^b = \begin{bmatrix} 1 & 0 & 0 & 0 \\ 0 & -1 & 0 & 0 \\ 0 & 0 & -1 & 0 \\ 0 & 0 & 0 & 1 \end{bmatrix} \tag{1}$$

The position and orientation of the frame fixed to the  $i$ th link can be easily found with the composition rule of homogeneous transformation matrices:

$$\mathbf{T}_i^b(q_1, \dots, q_i) = \begin{bmatrix} \mathbf{R}_i^{i-1} & \mathbf{p}_i^{i-1} \\ \mathbf{0} & 1 \end{bmatrix} = \begin{bmatrix} r_i^{i-1}{}_{11} & r_i^{i-1}{}_{12} & r_i^{i-1}{}_{13} & p_i^{i-1}{}_x \\ r_i^{i-1}{}_{21} & r_i^{i-1}{}_{22} & r_i^{i-1}{}_{23} & p_i^{i-1}{}_y \\ r_i^{i-1}{}_{31} & r_i^{i-1}{}_{32} & r_i^{i-1}{}_{33} & p_i^{i-1}{}_z \\ 0 & 0 & 0 & 1 \end{bmatrix} = \mathbf{T}_0^b \mathbf{T}_1^0(q_1) \dots \mathbf{T}_i^{i-1}(q_i) \tag{2}$$

where  $q_i$  is the  $i$ th generalised coordinate and  $T_i^{i-1}$  is the so-called homogeneous transformation matrix of frame  $i$  with respect to frame  $\{i - 1\}$  that can be computed as a function of the DH parameter and  $q_i$ :

$$\mathbf{T}_i^{i-1} = \begin{bmatrix} \cos(q_i) & -\cos(\alpha_i) \sin(q_i) & \sin(\alpha_i) \sin(q_i) & a_i \cos(q_i) \\ \sin(q_i) & \cos(\alpha_i) \cos(q_i) & -\sin(\alpha_i) \cos(q_i) & a_i \sin(q_i) \\ 0 & \sin(\alpha_i) & \cos(\alpha_i) & d_i \\ 0 & 0 & 0 & 1 \end{bmatrix} \tag{3}$$

where, in the following, the compact notation  $s_i = \sin(q_i)$  and  $c_i = \cos(q_i)$  is also used.

### 2.1. Swivel Angle Approach

To face the inverse kinematics problem and compute the posture (or, in general, the postures) that is consistent with a specified end-effector pose, the serial kinematic chain that forms the manipulator can be represented as the composition of two spherical joints linked by a revolute joint. Indeed, as shown in Fig. 4, the axes of the first three joints intersect at a single point named  $p_s$ , where  $s$  stands for ‘‘shoulder,’’ and the axes of the last three joints meet in  $p_w$ , since the manipulator wrist is spherical. In analogy with the human arm, the central joint represents therefore the elbow mobility, and the kinematic (or intrinsic) redundancy of the manipulator can be addressed by evaluating the elbow centre point  $p_e$  when  $p_s$  and  $p_w$  are fixed, leading to the so-called elbow angle or swivel angle approach. Since the spherical wrist joint is accountable for the end-effector frame  $\{7\}$  orientation, its position is instead ruled by the first four revolute joints that allow the rotation of the elbow point  $p_e$  along a circle  $S$  of radius  $R$  (Fig. 5).

It is worth noticing that the swivel circle  $S$  can be seen as the intersection of two cones that have  $p_e$  and  $p_w$  as their respective vertices, while the apothems depend on the geometric parameters  $D_1, D_2, D_3, D_4$  and  $e_2$ . In detail, while the apothem  $L$  of the cone with vertex in  $p_s$  is  $U = D_1 + D_2$ , the geometric off-set  $e_2$  causes a misalignment in the serial kinematic chain, thus the apothem of the second cone does not coincide with the sum  $D_3 + D_4$ . By observing Fig. 6, it is quite straightforward that, by defining:

$$L = D_3 + D_4 \tag{4}$$

the apothem of the cone with  $p_w$  as vertex can be computed as

$$L_{\perp} = \sqrt{L^2 + e_2^2} \tag{5}$$

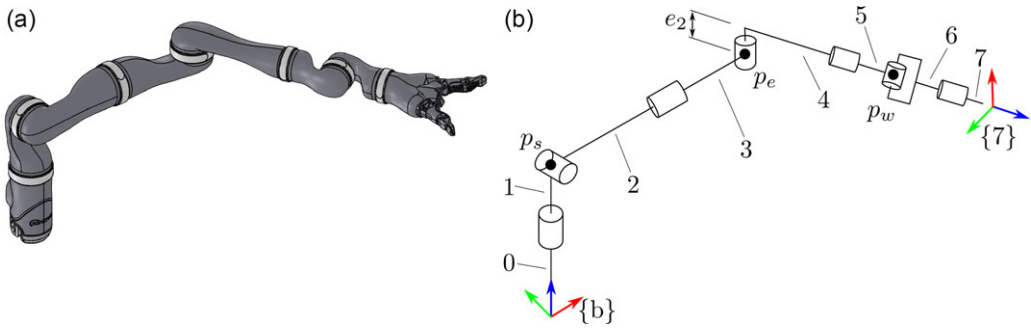


**Figure 4.** Modelling of the Kinova Jaco2 Manipulator as a composition of two spherical joints with an intermediate revolute joint. (a) 3D manipulator model, (b) Kinematic model.

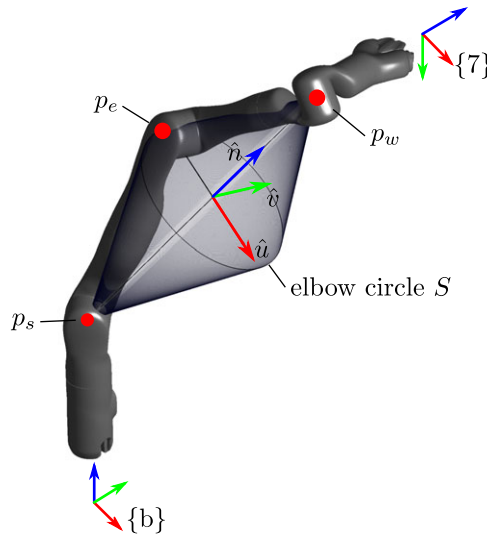


**Figure 5.** Rotation of the elbow point  $p_e$  along the swivel circle  $S$  of radius  $R$ .

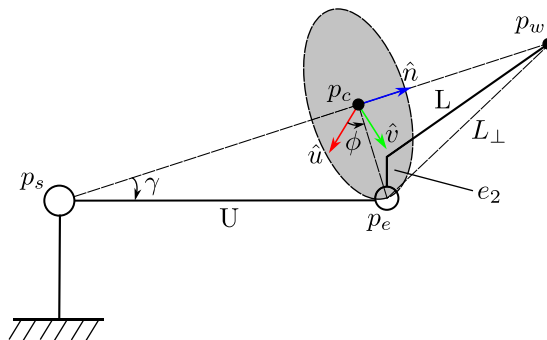


**Figure 6.** Representation of the characteristic parameters of the elbow angle IK approach.

Thus, to make use of the elbow angle approach, the position of the wrist centre  $p_w$  can be derived as follows:

$$\mathbf{p}_w = \mathbf{p}_7^b - (D_6 + D_7) [r_{713}^b \quad r_{723}^b \quad r_{733}^b] \tag{6}$$

where  $\mathbf{p}_7^b$  is the given goal position of the end-effector frame with respect to  $\{b\}$  and  $[r_{713}^b \quad r_{723}^b \quad r_{733}^b]$  is the third unit vector of the reference frame. To compute the  $\{\hat{\mathbf{u}}, \hat{\mathbf{v}}, \hat{\mathbf{n}}\}$  triplet, the following approach can be used:

$$\hat{\mathbf{n}} = \frac{\mathbf{p}_w - \mathbf{p}_s}{|\mathbf{p}_w - \mathbf{p}_s|} \tag{7}$$

$$\hat{\mathbf{u}} = \frac{\hat{\mathbf{u}} - (\hat{\mathbf{u}} \cdot \hat{\mathbf{n}}) \hat{\mathbf{n}}}{|\hat{\mathbf{u}} - (\hat{\mathbf{u}} \cdot \hat{\mathbf{n}}) \hat{\mathbf{n}}|} \tag{8}$$

$$\hat{\mathbf{v}} = \hat{\mathbf{n}} \wedge \hat{\mathbf{u}} \tag{9}$$

where  $\hat{\mathbf{a}}$  is an arbitrarily defined unit vector and the underlined notation defines the position vector with respect to the  $\{b\}$  frame. It is worth underlining that  $\hat{\mathbf{n}}$  is by definition perpendicular to the swivel circle  $S$ . The  $\gamma$  angle, i.e. the semi-vertical angle of the cone with  $p_s$  as the vertex, can be computed using the law of cosines with the two triangles  $p_s, p_c, p_e$  and  $p_c, p_e$  and  $p_w$ :

$$\gamma = \cos^{-1} \left( \frac{U^2 + |\mathbf{p}_w - \mathbf{p}_s|^2 - L_{\perp}^2}{2 |\mathbf{p}_w - \mathbf{p}_s| U} \right) \tag{10}$$

The position vector  $\mathbf{p}_c$  of the swivel circle centre and its radius  $R$  can be easily computed:

$$\mathbf{p}_c = \mathbf{p}_s + U \cos(\gamma) \hat{\mathbf{n}} \tag{11}$$

$$R = U \sin(\gamma) \tag{12}$$

The position vector of the elbow point  $\mathbf{p}_e$  can now be defined as a function of the derived parameters and the swivel angle  $\phi$ , i.e. the angle formed between  $\hat{\mathbf{u}}$  and  $\mathbf{p}_e - \mathbf{p}_c$ , and thus it represents the intrinsic kinematic redundancy of the manipulator:

$$\mathbf{p}_e = \mathbf{p}_c + R (\cos(\phi) \hat{\mathbf{u}} + \sin(\phi) \hat{\mathbf{v}}) \tag{13}$$

### 2.2. Joint Angles Computation

Once the position vector  $p_e$  has been computed as function of the swivel angle parameter  $\phi$ , its value can be used to compute the first two joint angles  $q_1$  and  $q_2$ . Indeed, by referring to the homogeneous transformation matrix  $\mathbf{T}_3^b$  that describes the position and orientation of the reference frame  $\{3\}$  with respect to  $\{b\}$ , the following applies:

$$\mathbf{T}_3^b = \mathbf{T}_0^b \mathbf{T}_1^0 \mathbf{T}_2^1 \mathbf{T}_3^2 = \begin{bmatrix} s_1 s_3 + c_1 c_2 c_3 & c_1 s_2 & c_3 s_1 - c_1 c_2 s_3 & c_1 s_2 (D_2 + D_3) \\ c_1 s_3 - c_2 c_3 s_1 & -s_1 s_2 & c_1 c_3 + c_2 s_1 s_3 & -s_1 s_2 (D_2 + D_3) \\ c_3 s_2 & -c_2 & -s_2 s_3 & D_1 - c_2 (D_2 + D_3) \\ 0 & 0 & 0 & 1 \end{bmatrix} \tag{14}$$

Since  $\mathbf{p}_e = \mathbf{p}_3^b$ , it is possible to compute the first two joint angles as follows:

$$q_1 = -\tan^{-1} \left( \frac{p_{3y}^b}{p_{3x}^b} \right) \tag{15}$$

$$q_2 = \tan^{-1} \left( \frac{\sqrt{p_{3x}^b{}^2 + p_{3y}^b{}^2}}{D_1 - p_{3z}^b} \right) \tag{16}$$

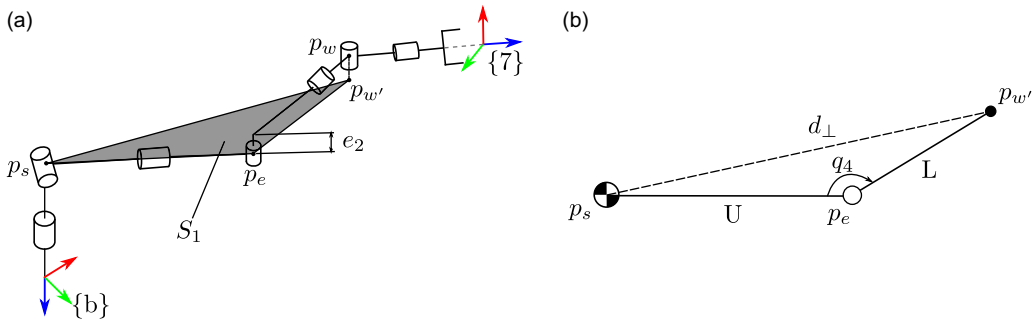


**Figure 7.** (a) Computation of the elbow angle  $q_4$  through geometric construction. (b) The wrist centre point  $p_w$  is projected onto the  $S_1$  plane.

The third joint value  $q_3$  can be calculated by imposing the following identity:

$$\mathbf{p}_e - e_2 \begin{bmatrix} r_{313}^b & r_{323}^b & r_{333}^b \end{bmatrix} = \mathbf{p}_w + L \begin{bmatrix} r_{413}^b & r_{423}^b & r_{433}^b \end{bmatrix} \tag{17}$$

where  $\begin{bmatrix} r_{313}^b & r_{323}^b & r_{333}^b \end{bmatrix}$  and  $\begin{bmatrix} r_{413}^b & r_{423}^b & r_{433}^b \end{bmatrix}$  are the third components of the reference frames {3} and {4} that can be extracted from their respective homogeneous transformation matrices:

$$\begin{bmatrix} r_{313}^b & r_{323}^b & r_{333}^b \end{bmatrix} = \begin{bmatrix} c_3 s_1 - c_1 c_2 s_3 & c_1 c_3 + c_2 s_1 s_3 & -s_2 s_3 \end{bmatrix} \tag{18}$$

$$\begin{bmatrix} r_{413}^b & r_{423}^b & r_{433}^b \end{bmatrix} = \begin{bmatrix} -s_4(c_1 c_2 c_3 + s_1 s_3) + c_4(c_1 s_2) \\ -s_4(s_1 c_2 c_3 + c_1 s_3) + c_4(-s_1 s_2) \\ -s_4 s_2 c_3 - c_4 c_2 \end{bmatrix} \tag{19}$$

Even though Eq. (17) is function of  $q_3$  but also  $q_4$ , it can still be solved since  $q_4$ , i.e. the elbow angle, can be directly computed through geometric construction. As presented in Fig. 7(a), the  $p_w$  point can be translated with a fixed off-set  $e_2$  along the  $e_2$  direction, thus obtaining the point  $p_{w'}$ . Looking at the  $\{p_s, p_e, p_{w'}\}$  triangle on the  $S_1$  plane, Fig. 7(b), the value of the elbow joint  $q_4$  can be easily obtained through the cosine law:

$$q_4 = \cos^{-1} \left( \frac{L^2 + U^2 - d_{\perp}^2}{2UL} \right) \tag{20}$$

where

$$d_{\perp} = \sqrt{|\mathbf{p}_w - \mathbf{p}_s|^2 + e_2^2} \tag{21}$$

$q_3$  can now be computed as

$$c_3 = - \frac{e_2 s_2 p_{wx} - e_2 s_2 p_{ex} + c_1 c_2 e_2 p_{ez} - c_1 c_2 e_2 p_{wz}}{s_2 (s_1 L^2 s_4^2 + s_1 e_2^2)} + \frac{+L s_1 s_4 p_{ez} - L s_1 s_4 p_{wz} + L c_1 c_2^2 c_4 e_2 + L c_1 c_4 e_2 s_2^2 + L^2 c_2 c_4 s_1 s_4}{s_2 (s_1 L^2 s_4^2 + s_1 e_2^2)} \tag{22a}$$



$$s_3 = \frac{e_2 s_1 p_{wz} - e_2 s_1 p_{ez} - L s_2 s_4 p_{ex} + L s_2 s_4 p_{wx} + L^2 c_1 c_2^2 c_4 s_4}{s_2 (s_1 L^2 s_4^2 + s_1 e_2^2)} \tag{22b}$$

$$\frac{+L^2 c_1 c_4 s_2^2 s_4 - L c_2 c_4 e_2 s_1 + L c_1 c_2 s_4 p_{ez} - L c_1 c_2 s_4 p_{wz}}{s_2 (s_1 L^2 s_4^2 + s_1 e_2^2)}$$

$$q_3 = \tan^{-1} \left( \frac{s_3}{c_3} \right) \tag{22c}$$

Regarding the values of the last three joint angles, the standard inverse kinematics procedure for spherical joint was applied, thus by evaluating the  $T_7^4$  homogeneous transformation matrix:

$$T_7^4 = T_b^4 T_7^b \tag{23}$$

where

$$T_b^4 = \begin{bmatrix} R_4^{bT} & -R_4^{bT} P_4^b \\ [0, 0, 0] & 1 \end{bmatrix} \tag{24}$$

Finally,  $q_5, q_6, q_7$  can be computed:

$$q_5 = \tan^{-1} \left( \frac{r_{7\ 23}^4}{r_{7\ 13}^4} \right) \tag{25}$$

$$q_7 = \tan^{-1} \left( \frac{-r_{7\ 32}^4}{-r_{7\ 31}^4} \right) \tag{26}$$

$$q_6 = \tan^{-1} \left( \frac{r_{7\ 32}^4}{\sin(q_7)} \right) \tag{27}$$

### 2.3. Redundancy Evaluation

Since the swivel angle approach is a closed-form solution of the inverse kinematics problem for the Jaco2 manipulator, it can be used to extract the entire range of possible postures that corresponds to a given goal pose  $T_7^b$ . Indeed, it is worth noticing the manipulator joint space has size  $m = 7$  while its workspace has size  $n = 6$ , thus the arm has  $m - n = 1$  degree of kinematic redundancy. Typically, this feature is exploited to augment the mobility of the manipulator, e.g. for collision avoidance algorithms. The typical behaviour of the joint angle values as a function of the swivel angle  $\phi$  is presented in Fig. 8, where the curves are presented in the range  $[0, 2\pi]$ . Focusing on joint 6 curve, the whole set of possible solutions is restricted due to the physical joint limit constraints that impose a minimum admitted value on  $q_6$ . In general, the Kinova Jaco2 manipulator presents physical joint limits in joint 2, 4, 6, as presented in Table III. Thus, it seems evident that the closed-form solution can also be exploited to avoid those solutions that are outside or even close to the admitted joint values boundary. To this aim, Vahrenkamp et al. [25] presented a novel approach in which an extended manipulability index, which takes into account closeness to joint limits and possible obstacles, is presented.

Starting from Togai’s definition of manipulability index [26], that estimates the posture closeness to kinematic singularities:

$$c(\mathbf{J}) = \frac{1}{\text{cond}(\mathbf{J})} = \frac{\lambda_{\min}}{\lambda_{\max}} \tag{28}$$

where  $\mathbf{J} = \mathbf{J}(q_1, \dots, q_7)$  is the arm Jacobian matrix and  $\lambda_{\min, \max}$  are its minimum and maximum eigenvalues, in refs. [25, 27] the following penalisation function  $p_j$  for the  $j$ th column of the Jacobian is presented:

**Table III.** Physical joint limit values for Kinova Jaco2 manipulator.

$q$	$q_{\min}$ (deg)	$q_{\max}$ (deg)
2	47	313
4	30	330
6	65	295

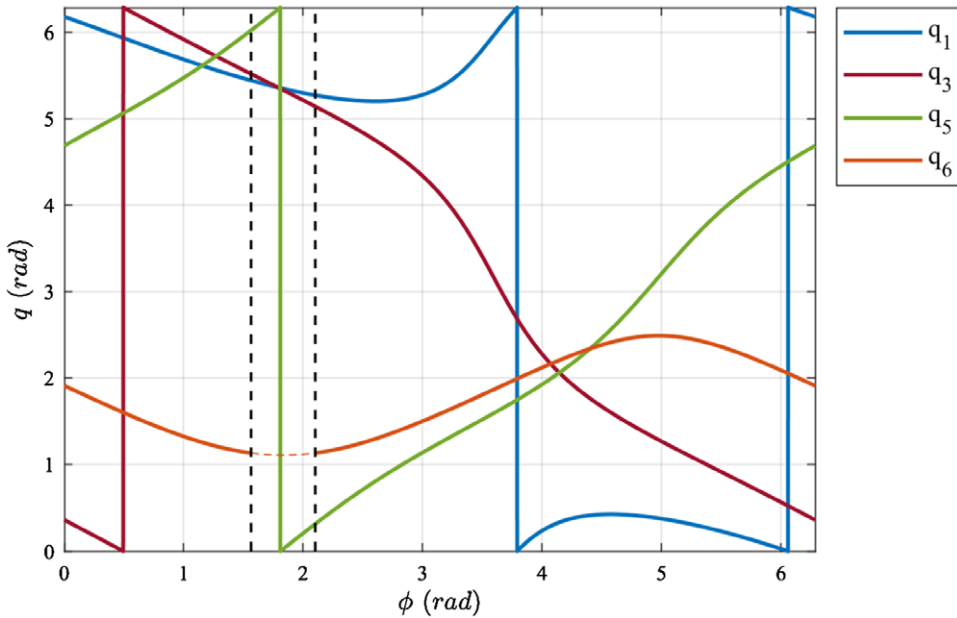


**Figure 8.** Behaviour of the values of the joint angles in the interval  $[0, 2\pi]$  as a function of the swivel angle  $\phi$  for a given pose. The black vertical dotted lines demarcate the not allowed solutions due to joint 6 limit constraints.

$$p_j = \frac{1}{\sqrt{1 + |\nabla h(q_j)_j|}} \tag{29a}$$

$$\nabla h(q_j) = \frac{(\theta_{j,\max} - \theta_{j,\min})^2 (2\theta_j - \theta_{j,\max} - \theta_{j,\min})^2}{\xi (\theta_{j,\max} - \theta_j)^2 (\theta_j - \theta_{j,\min})^2} \tag{29b}$$

where  $q_{j,\max}, q_{j,\min}$  were presented in Table III and  $\xi$  is an arbitrarily defined parameter that accentuates or relaxes the  $p_j$  function. In detail, it is easy to check that larger values of  $\xi$  increase the area where  $p_j$  has a value close to one. In this paper, the value of  $\xi = 4$ , as used in ref. [25], was selected.

The manipulability  $c$  can then be modified into  $c_{\text{mod}}$  evaluating the condition number of the modified Jacobian, where the  $j$ th column of the matrix is multiplied with the corresponding penalisation factor  $p_j$ :

$$J_{\text{mod},j} = J_{ij}p_j \quad i = 1, \dots, 6, j = 1, \dots, 7 \tag{30}$$

The behaviour of  $c$  and  $c_{\text{mod}}$  is presented in Fig. 9, where the closeness to the joint 6 physical limit leads to a significant penalisation of  $c$ . The implementation of the manipulability index  $c_{\text{mod}}$  therefore establishes a criterion to evaluate the “best” posture that corresponds to a defined goal pose, thus allowing to extract a solution from the inverse kinematics set presented in Fig. 8.

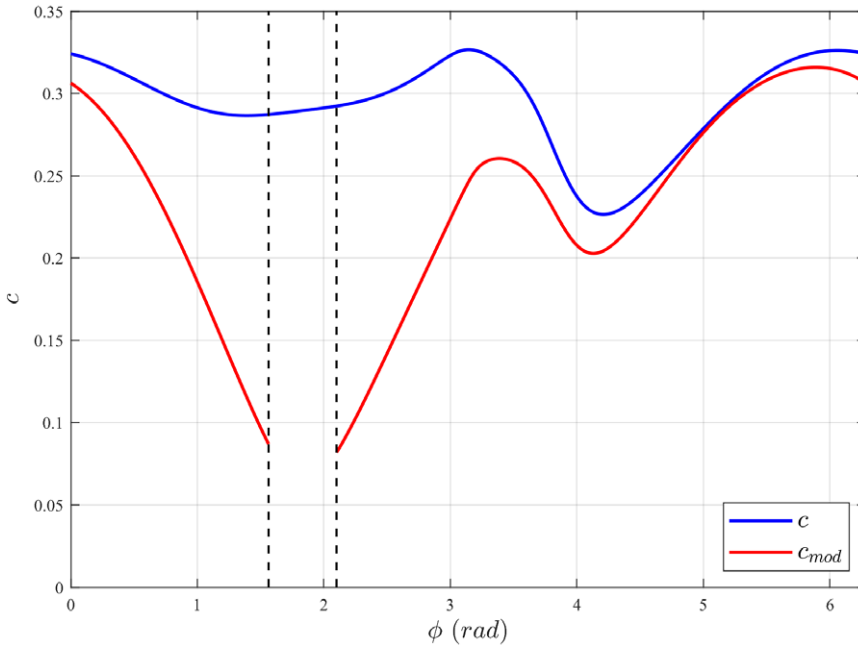


**Figure 9.** Manipulability index as a function of the elbow angle for a defined goal pose. Vertical dashed lines denote the area not allowed due to joint limit constraints.

### 3. System Implementation

To properly navigate and collect crops, the manipulator mobility can be augmented thanks to Agri.Q kinematics, i.e. the mobile base mobility, thus making the whole system a mobile manipulator. Even though the Agri.Q mobility is quite complex, due to the articulated architecture and the potential eight drive wheels, as presented by the authors in refs. [28, 29], its kinematics is here simplified for crop collecting purposes that can be classified as pick-and-place tasks.

When navigating inside vineyard rows, the two degrees of freedom that can be used to augment the manipulator mobility are the linear displacement  $x$  and the pitch angle  $\psi$ , as presented in Fig. 10. While it is quite straightforward to understand the impact of  $x$ , it is worth underlining that the pitch angle has the double effect of moving the arm upwards but also rotating it.

Even though several motion planning algorithms extend the Jacobian of the arm with the base one, thus moving towards the simultaneous motion of the base and the arm [30, 31], the motion planning is here addressed with the decoupling of the mobile base motion and the manipulator one, due to the significant difference between the position accuracy of the two systems. According to this approach, the linear displacement  $x$  and the pitch angle  $\psi$  are used to position the manipulator near the goal grape peduncle, then the arm is used to perform the pick and place task. Since the base mobility cannot affect the displacement of a grape along the  $y$  axis of  $\{b\}$ , the base can translate and rotate the arm workspace (Fig. 11) to position the goal point inside the area where the manipulability index  $c_{mod}$  has the highest value [28].

It is worth underlining that, although it significantly simplifies the motion planning pipeline, the proposed approach cannot be used for dynamic handling or grasping, since it is mainly based on a static representation of the environment and the Agri.Q itself. It is also assumed that the Agri.Q base can fulfill the arm positioning task with the theoretical absence of positioning errors, which is quite impossible to obtain in a real vineyard. This aspect is partially compensated since the target point is positioned inside the area where the Jaco2 manipulator presents the highest value of manipulability index. Thus, if the positioning error is restricted, the target point still lies into the best manipulability area. Nonetheless,

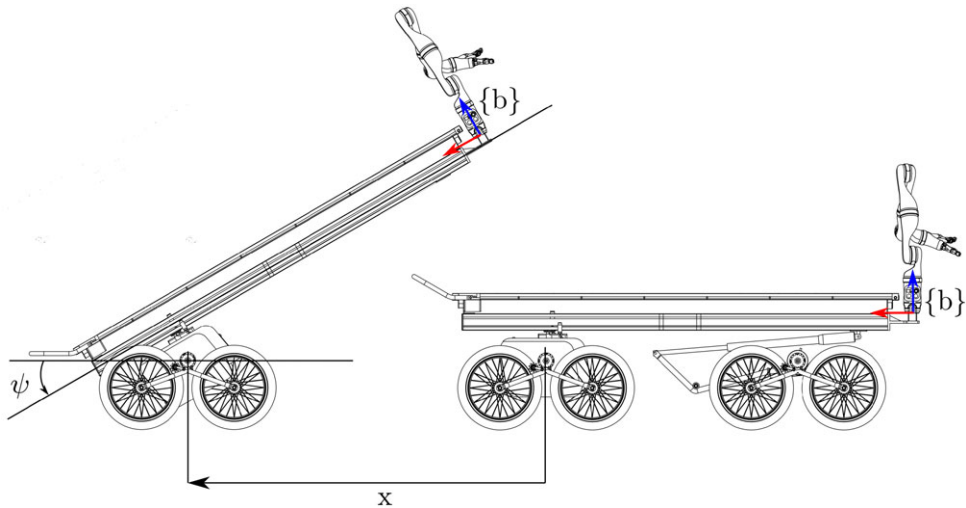


Figure 10. Agri.Q base mobility simplification for crop sampling.

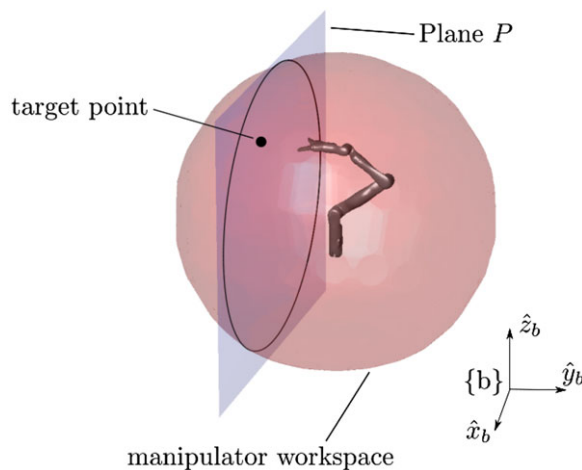


Figure 11. Use of the Agri.Q mobility to translate and rotate the arm workspace. Plane P is parallel to  $\langle \hat{x}_b, \hat{z}_b \rangle$  and its displacement along  $\hat{y}_b$  is established by the position of the target point.

the evaluation of the cited area depends on the pose of the target object, i.e. its position along the  $y$  axis of  $\{b\}$  and its orientation, so it would be outperformed for each target grapevine, with a significant increment in the overall computational time.

### 3.1. Software Development

Within the present sub-section, a comprehensive description of the developed software architecture for the system control is presented.

Regarding the closed-form inverse kinematics method presented in Section 2, the developed algorithm is hereafter reported in pseudo-code form in Algorithm 1. Since it can be potentially used for different research activities, the IK code is provided as open-source Matlab code by the authors.<sup>1</sup> The library was developed using the Matlab multidimensional matrices functionality, to optimise the

<sup>1</sup><https://github.com/gicolucci/Jaco2SwivelIK>

**Algorithm 1. Inverse kinematics elbow angle algorithm**


---

```

angle ← [α, β, γ]                                ▶ The tool center point represented as XYZ Euler angles

T7goalb ← eul2tform(angle, 'XYZ')                ▶ The goal T7b 4x4 homogeneous transformation matrix

T7goalb(1 : 3, 4) ← [px, py, pz]                ▶ The tool center point goal position is inserted into T7b

SwivelIKOption ← 'Fixed' or 'Optimized' or 'All';    ▶ To identify the IK algorithm output

if SwivelIKOption = 'Fixed' then                ▶ The solution at a given elbow angle φ is computed
    φ ← φgoal
    pe ← pc + R cos(φ) ũ + R sin(φ) ũ;                ▶ pe is a 1x3 vector
    q ← Solveq(pe, T7goalb);                ▶ The output is a 7x1 joint angles vector
else if SwivelIKOption = 'Optimize' or 'All' then
    φ ← linspace(0, 2π, npoints); ▶ The continuous set of solutions is discretized into npoints values
    pe ← pc + R cos(φ) ũ + R sin(φ) ũ;                ▶ pe is a npointsx3 matrix
    q ← Solveq(pe, T7goalb);
    Compute Jmod taking into account the penalization factors
    for counter = 1 : npoints do
        if the posture is feasible then
            cmod(counter) ←  $\frac{1}{\text{cond}(\mathbf{J}_{\text{mod}}(:, :, \text{counter}))}$ ;
        else if the physical joint limit constraints don't allow the posture then
            cmod(counter) ← 0;
        end if
    end for
    if SwivelIKOption = 'Optimize' then ▶ The solution at which corresponds the biggest cmod
    value is computed
        [cmodmax, index] ← max(cmod);
        q ← q(index, :);                ▶ The output is a 7x1 joint angles vector
    else if SwivelIKOption = 'All' then ▶ The whole set of solution, discretized according to the
    φ elbow angle vector definition, is computed
        q ← q                ▶ The output is a 7xnpoints joint angles matrix
        cmod ← cmod
    end if
end if

```

---

computation time especially in case of redundancy evaluation, where a significant reduction of the computational cost from the average value of 0.65s to 0.15s was obtained.<sup>2</sup> The code was further optimised with the Matlab .mex code generation functionality, where the average computation time of 0.09 s was achieved.<sup>3</sup> The code uses the *Solveq* sub-function that performs the joint angles computation according to Subsection 2.2.

<sup>2</sup>Tested on a Dell XPS machine, with Ubuntu 20.04 LTS, and an Intel i7-10510U@1.80 GHz processor. The computation time is evaluated as the average of 20 tests.

<sup>3</sup>If requested, the .mex file can be provided by the authors.

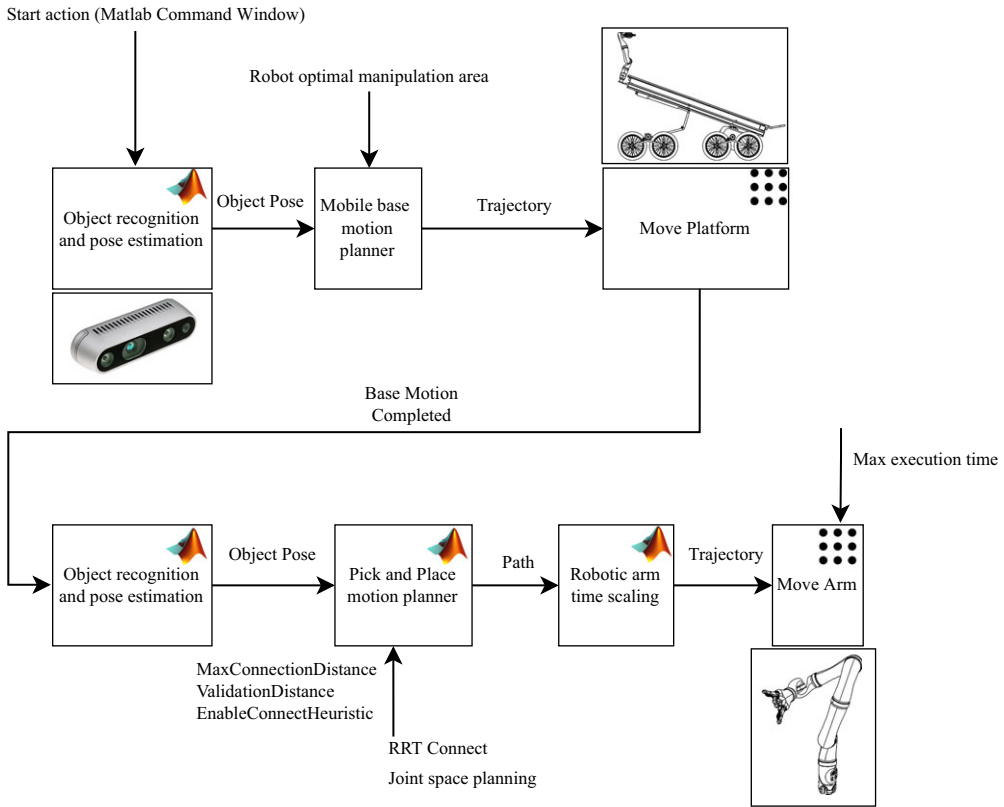


**Figure 12.** Software system architecture. The Matlab and ROS logo are used to indicate the selected environment for a specific block.

Regarding the Agri.Q system implementation, in Fig. 12 a representation of a first and simplified system software architecture is presented, where the interaction between Matlab and ROS environment was done through the Matlab ROS Toolbox [32]. A camera block will be implemented for object recognition and pose estimation of the target, i.e. the grape peduncle, both before and after the mobile base motion to avoid possible positioning errors of the mobile base, while the manipulator path planning pipeline involves the use of standard sample-based joint space path planning like RRT connect [33]. Except for the camera block, the presented pipeline was used to perform a first laboratory experimental validation, as shown in Fig. 13. Agri.Q was able to pick-and-place a grapevine sample.

#### 4. Conclusions

Within this paper, the development and implementation of the motion planning pipeline for Agri.Q mobile manipulator for PA were presented. The algorithm had integrated the resolution of the arm kinematic redundancy through the closed-form elbow angle formulation, that is provided by the author as an open source Matlab code. The whole system motion pipeline was instead addressed using a motion decoupling approach, where the mobile base translates and rotates the manipulator workspace to position the goal point inside the area with the highest value of the manipulability index. The whole architecture was implemented on the real prototype and validated through first tests in laboratory environment. As further developments, a perception block will be developed to both recognise the target peduncle and also provide a feedback after the mobile base motion to correct possible positioning errors.

**Acknowledgements.** The authors gratefully thank the Pic4Ser - PoliTO Interdepartmental Centre For Service Robotics. <https://pic4ser.polito.it/>.

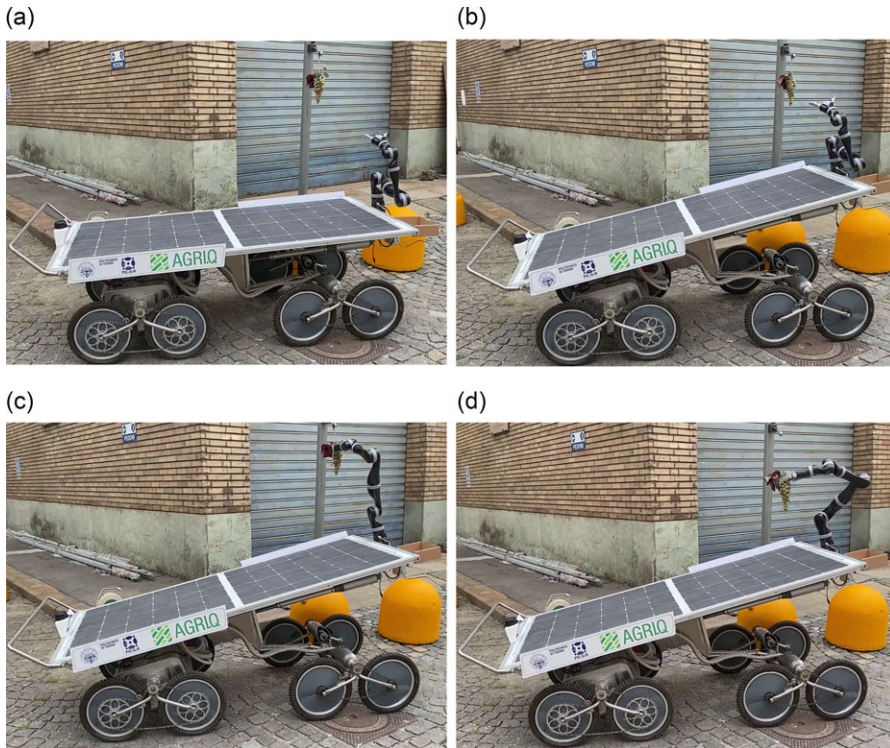


**Figure 13.** *Agri.Q* prototype first experimental tests. (a) Rest configuration, (b) goal peduncle approach, (c) peduncle picking, (d) place of the peduncle.

**Author contributions.** GC, AB, LT and GQ conceived and designed the study. GC, LT and AB carried out the software implementation. GQ validated the study. GC and AB prepared the draft of the paper. GQ, LT and LB edited and reviewed the draft.

**Financial support.** This research received no specific grant from any funding agency, commercial or not-for-profit sectors.

**Conflicts of interest.** The authors declare no conflicts of interest exist.

**Ethical approval.** Not applicable.

## References

- [1] S. A. Kumar and P. Ilango, “The impact of wireless sensor network in the field of precision agriculture: A review,” *Wirel. Pers. Commun.* **98**(1), 685–698 (2018). doi: [10.1007/s11277-017-4890-z](https://doi.org/10.1007/s11277-017-4890-z).
- [2] R. Bongiovanni and J. Lowenberg-Deboer, “Precision agriculture and sustainability,” *Precis. Agric.* **5**(4), 359–387 (2004). doi: [10.1023/B:PRAG.0000040806.39604.aa](https://doi.org/10.1023/B:PRAG.0000040806.39604.aa).
- [3] A. T. Meshram, A. V. Vanalkar, K. B. Kalambe and A. M. Badar, “Pesticide spraying robot for precision agriculture: A categorical literature review and future trends,” *J. Field Robot.* **39**(2), 153–171 (2022). doi: [10.1002/rob.22043](https://doi.org/10.1002/rob.22043).
- [4] United Nations, Department of Economic and Social Affairs, Population Division, “World Population Prospects 2022: Summary of Results,” In: *UN DESA/POP/2022/TR/NO. 3* (2022).
- [5] F. J. Pierce and P. Nowak, “Aspects of Precision Agriculture,” In: *Advances in Agronomy* (Sparks D. L., ed.) (Academic Press, New York, 1999) pp. 1–85. [10.1016/S0065-2113\(08\)60513-1](https://doi.org/10.1016/S0065-2113(08)60513-1).
- [6] E. Crist, C. Mora and R. Engelman, “The interaction of human population, food production, and biodiversity protection,” *Science* **356**(6335), 260–264 (2017). doi: [10.1126/science.aal2011](https://doi.org/10.1126/science.aal2011).
- [7] T. W. Griffin and E. A. Yeager, “How Quickly Do Farmers Adopt Technology? A Duration Analysis,” In: *Precision Agriculture’19* (2019).
- [8] Oliver M., Bishop T. and Marchant B. (Eds.). *Precision Agriculture for Sustainability and Environmental Protection* (1st ed.) (Routledge, Abingdon, 2013). [10.4324/9780203128329](https://doi.org/10.4324/9780203128329).

- [9] SDG 12. *Ensure Sustainable Consumption and Production Patterns* (n.d.). <https://sdgs.un.org/goals/goal12> (accessed November 13, 2022).
- [10] J. T. F. Rosas, F. A. de Carvalho Pinto, D. M. de Queiroz, F. M. de Melo Villar, D. S. M. Valente and R. N. Martins, “Coffee ripeness monitoring using a UAV-mounted low-cost multispectral camera,” *Precis. Agric.* **23**(1), 300–318 (2022). doi: [10.1007/s11119-021-09838-3](https://doi.org/10.1007/s11119-021-09838-3).
- [11] K. Mikula, G. Izydorczyk, D. Skrzypczak, M. Mironiuk, K. Moustakas, A. Witek-Krowiak and K. Chojnacka, “Controlled release micronutrient fertilizers for precision agriculture - A review,” *Sci. Total Environ.* **712**, 136365 (2020). doi: [10.1016/j.scitotenv.2019.136365](https://doi.org/10.1016/j.scitotenv.2019.136365).
- [12] A. Chawade, J. van Ham, H. Blomquist, O. Bagge, E. Alexandersson and R. Ortiz, “High-throughput field-phenotyping tools for plant breeding and precision agriculture,” *Agronomy* **9**(5), 258 (2019). doi: [10.3390/agronomy9050258](https://doi.org/10.3390/agronomy9050258).
- [13] N. Strisciuglio, R. Tylecek, N. Petkov, P. Bieber, J. Hemming, E. Henten, T. Sattler, M. Pollefeys, T. Gevers, T. Brox and R. B. Fisher. *TrimBot2020: An Outdoor Robot for Automatic Gardening* (2018).
- [14] Vinum Project. <https://vinum-robot.eu/> (accessed on 09 January 2023).
- [15] T. Botterill, S. Paulin, R. Green, S. Williams, J. Lin, V. Saxton, S. Mills, X. Chen and S. Corbett-Davies, “A robot system for pruning grape vines,” *J. Field Robot.* **34**(6), 1100–1122 (2017). doi: [10.1002/rob.21680](https://doi.org/10.1002/rob.21680).
- [16] G. Adamides, C. Katsanos, I. Constantinou, G. Christou, M. Xenos, T. Hadzilacos and Y. Edan, “Design and development of a semi-autonomous agricultural vineyard sprayer: Human-robot interaction aspects,” *J. Field Robot.* **34**(8), 1407–1426 (2017). doi: [10.1002/rob.21721](https://doi.org/10.1002/rob.21721).
- [17] J. Goričanec, N. Kapetanović, I. Vatavuk, I. Hrabar, G. Vasiljević, G. Gledec, D. Stuhne, S. Bogdan, M. Orsag, T. Petrović, N. Mišković, Z. Kovačić, A. Kurtela, J. Bolotin, V. Kožul, N. Glavič, N. Antolović, M. Anič, B. Kozina and M. Cukon, “Heterogeneous Autonomous Robotic System in Viticulture and Mariculture - Project Overview,” In: *2021 16th International Conference on Telecommunications* (2021) pp. 181–188. [10.23919/Con\\_TEL52528.2021.9495969](https://doi.org/10.23919/Con_TEL52528.2021.9495969).
- [18] Q. Feng, X. Wang, G. Wang and Z. Li, “Design and Test of Tomatoes Harvesting Robot,” In: *2015 IEEE International Conference on Information and Automation* (2015) pp. 949–952. [10.1109/ICInfA.2015.7279423](https://doi.org/10.1109/ICInfA.2015.7279423).
- [19] A. De Preter, J. Anthonis and J. De Baerdemaeker, “Development of a robot for harvesting strawberries,” *IFAC-PapersOnLine* **51**(17), 14–19 (2018). doi: [10.1016/j.ifacol.2018.08.054](https://doi.org/10.1016/j.ifacol.2018.08.054).
- [20] P. Cavallone, A. Botta, L. Carbonari, C. Visconte and G. Quaglia, “The Agri.q Mobile Robot: Preliminary Experimental Tests,” In: *Advances in Italian Mechanism Science* (V. Niola and A. Gasparetto, eds.) (Springer, Cham, 2021) pp. 524–532. [10.1007/978-3-030-55807-9\\_59](https://doi.org/10.1007/978-3-030-55807-9_59).
- [21] A. Botta and P. Cavallone, “Robotics Applied to Precision Agriculture: The Sustainable Agri.q Rover Case Study,” In: *Proceedings of I4SDG Workshop 2021* (Quaglia G., Gasparetto A., Petuya V. and Carbone G., ed.) (Springer, Cham, 2022) pp. 41–50. [10.1007/978-3-030-87383-7\\_5](https://doi.org/10.1007/978-3-030-87383-7_5).
- [22] G. Colucci, L. Baglieri, A. Botta, P. Cavallone and G. Quaglia, “Optimal Positioning of Mobile Manipulators Using Closed Form Inverse Kinematics,” In: *International Conference on Robotics in Alpe-Adria Danube Region* (Springer, Cham, 2022) pp. 184–191.
- [23] J. Baillieul, J. Hollerbach and R. Brockett, “Programming and Control of Kinematically Redundant Manipulators,” In: *The 23rd IEEE Conference on Decision and Control* (1984) pp. 768–774. [10.1109/CDC.1984.272110](https://doi.org/10.1109/CDC.1984.272110).
- [24] Kinova Gen2 User Guide. <https://drive.google.com/file/d/1XqbKx1-v3SfAentKR9f3p3c2SVdViyQl/view> (accessed on 5 November 2022).
- [25] N. Vahrenkamp, T. Asfour, G. Metta, G. Sandini and R. Dillmann, “Manipulability Analysis,” In: *12th IEEE-RAS International Conference on Humanoid Robots (Humanoids 2012)* (IEEE, Osaka, Japan, 2012) pp. 568–573. [10.1109/HUMANOIDS.2012.6651576](https://doi.org/10.1109/HUMANOIDS.2012.6651576).
- [26] M. Togai, “An application of the singular value decomposition to manipulability and sensitivity of industrial robots,” *SIAM J. Algebr. Discrete Methods* **7**(2), 315–320 (1986). doi: [10.1137/0607034](https://doi.org/10.1137/0607034).
- [27] F. Chen, M. Selvaggio and D. G. Caldwell, “Dexterous grasping by manipulability selection for mobile manipulator with visual guidance,” *IEEE Trans. Ind. Inform.* **15**(2), 1202–1210 (2019). doi: [10.1109/TII.2018.2879426](https://doi.org/10.1109/TII.2018.2879426).
- [28] G. Colucci, A. Botta, L. Tagliavini, P. Cavallone, L. Baglieri and G. Quaglia, “Kinematic modeling and motion planning of the mobile manipulator Agri.Q for precision agriculture,” *Machines* **10**(5), 321 (2022). doi: [10.3390/machines10050321](https://doi.org/10.3390/machines10050321).
- [29] L. Carbonari, A. Botta, P. Cavallone, L. Tagliavini and G. Quaglia, “Data-driven analysis of locomotion for a class of articulated mobile robots,” *J. Mech. Robot.* **13**(5), (2021). doi: [10.1115/1.4051018](https://doi.org/10.1115/1.4051018).
- [30] A. De Luca, G. Oriolo and P. R. Giordano, “Kinematic Modeling and Redundancy Resolution for Nonholonomic Mobile Manipulators,” In: *Proceedings 2006 IEEE International Conference on Robotics and Automation* (2006) pp. 1867–1873. [10.1109/ROBOT.2006.1641978](https://doi.org/10.1109/ROBOT.2006.1641978).
- [31] F. Neri, C. Scoccia, L. Carbonari, G. Palmieri, M. Callegari, L. Tagliavini, G. Colucci and G. Quaglia, “Dynamic Obstacle Avoidance for Omnidirectional Mobile Manipulators,” In: *Advances in Italian Mechanism* (V. Niola, A. Gasparetto, G. Quaglia and G. Carbone, eds.) (Springer, Cham, 2022) pp. 746–754. [10.1007/978-3-031-10776-4\\_86](https://doi.org/10.1007/978-3-031-10776-4_86).
- [32] Mathworks. *ROS Toolbox*. <https://it.mathworks.com/products/ros.html> (accessed November 13, 2022).
- [33] J. J. Kuffner and S. M. LaValle, “RRT-Connect: An Efficient Approach to Single-Query Path Planning,” In: *Proceedings 2000 ICRA. Millennium Conference, IEEE International Conference on Robotics and Automation*, vol. **2** (2000) pp. 995–1001. [10.1109/ROBOT.2000.844730](https://doi.org/10.1109/ROBOT.2000.844730).

**Cite this article:** G. Colucci, L. Tagliavini, A. Botta, L. Baglieri and G. Quaglia (2023). “Decoupled motion planning of a mobile manipulator for precision agriculture”, *Robotica* **41**, 1872–1887. <https://doi.org/10.1017/S0263574723000243>